Rational Design and Engineering of Quantum-Dot-Sensitized TiO_2 Nanotube Arrays for Artificial Photosynthesis

*Jungki Ryu, Sahng Ha Lee, Dong Heon Nam, and Chan Beum Park**

Redox enzymes can catalyze complex synthesis reactions under mild conditions but conventional catalysts rarely accomplish this task. Despite the high potential of redox enzymes for the synthesis of valuable compounds (e.g., chiral alcohols and drug intermediates),[1–5] their application is hampered by the high cost of enzyme-specific cofactors that are required as a redox equivalent, such as nicotinamide adenine dinucleotide (NAD(P)H) and flavin adenine dinucleotide (FADH). Thus, numerous efforts have been made over the past decades to accomplish in situ cofactor regeneration from their oxidized counterpart.[6–9] For example, researchers found that NAD(P)H can be successfully regenerated by introducing secondary enzymes[10–12] that reduce its oxidized counterpart (i.e., $NAD(P)^+$) or electrodes[13–15] with an external power supply into reaction media. However, these approaches present intrinsic drawbacks (e.g., by-product formation and requirement of secondary enzymes for biocatalytic regeneration, as well as extremely low yield and high overpotential for electrochemical regeneration) that hindered their practical application beyond the laboratory scale.[6–8]

Herein, we report on the development of quantum-dot-sensitized TiO_2 nanotube arrays for redox enzymatic synthesis coupled with the photoregeneration of nicotinamide cofactors via inspiration from natural photosynthesis. In natural photosynthesis,[16,17] incident light electronically excites a membrane-bound protein–pigment complexes called a photosystem. The photogenerated electrons are rapidly delivered to reaction centers along the electron transport chain for regenerating NADPH cofactors. These cofactors drive redox enzymatic reactions to synthesize organic compounds in the Calvin cycle. Its unique features (e.g., environmental compatibility and near-unity quantum yield) have fascinated scientists and provided inspiration to improve the efficiency of solar cells and photoelectrochemical hydrogen production systems.[18–24] In the present study, the photosystem for in situ NAD(P)H regeneration consisted of TiO_2–CdS nanotubes as a photoelectrode, triethanolamine (TEOA) as an electron donor, and pentamethylcyclopentadienyl rhodium bipyridine ($[Cp^*Rh(bpy)(H_2O)]^{2+}$) as an electron mediator and a hydride transfer catalyst (Figure S1, Supporting Information). As a photoelectrode for non-enzymatic regeneration of NAD(P)H, a nanotubular TiO_2–CdS film has many advantages that include easy synthesis and morphology control,[25,26] efficient charge separation,[24,27] and better diffusion of reaction species through nanotube channels. Due to the small size and more negative position of the conduction band (CB) edge of CdS compared to TiO_2 (at least 0.2 V more negative), photogenerated electrons can be rapidly injected from CdS to TiO_2 in a thermodynamically favorable manner (Figure S1, Supporting Information). This injection suppresses electron–hole recombination, which is more dominant than charge separation, especially in a nanometer-sized semiconductor particle.[24,27] Upon light irradiation, TEOA is oxidized at redox potential (E) $\approx -0.84 \pm 0.12$ V vs NHE; it donates electrons to CdS, preventing photocorrosion of CdS[18] and photodegradation of other organic components[28] by photogenerated holes in the valence band (VB) of CdS. Note that $[Cp^*Rh(bpy)(H_2O)]^{2+}$ can selectively regenerate enzymatically active 1,4-NAD(P)H among various NAD(P)H isomers and dimers by taking two electrons and one proton from the photoelectrode ($E \approx -0.5$ V) and stereoselectively transferring them to $NAD(P)^+$ ($E \approx -0.3$ V). The rhodium-based mediator can also regenerate other cofactors such as NADH with a phosphate group (i.e., NADPH) and FADH.[29,30]

The TiO_2–CdS nanotube (NT) film was prepared by anodizing Ti foil[25,26] followed by coating CdS nanoparticles through successive ionic layer adsorption and reaction (SILAR).[22] Scanning electron microscopy (SEM) images show that pristine TiO_2 nanotubes were well-aligned parallel to each other and perpendicular to the underlying Ti substrate (**Figure 1**a,b). The as-anodized TiO_2 nanotube film had an amorphous phase (Figure 1c) and exhibited a negligible absorbance in the visible light range (Figure 1d). The formation and growth of CdS nanoparticles during the SILAR process were readily identified by monitoring changes in the X-ray diffraction (XRD) pattern (Figure 1c), absorbance spectra (Figures 1d and Figure S2, Supporting Information), electron microscopy images (Figures 1a,b and Figures 1e,f), and elemental composition (Figure S3, Supporting Information). As shown in Table S1 (Supporting Information), the optical bandgap of the TiO_2–CdS nanotube film (estimated by Tauc's extrapolation method[31]), decreased with repeating the coating procedure. Such a decrease indicated the quantum confinement effect. Indeed, the size of the CdS nanoparticles (e.g., 2.36 nm after four cycles of SILAR process) was within the range exhibiting the quantum confinement effect for CdS less than 10 nm.[32]

The feasibility of the TiO_2–CdS nanocomposite film for photochemical NADH regeneration and enzymatic synthesis of organic compounds was tested (**Figure 2**). The experimental setup is shown in Figure 2c and explained in more detail in

J. Ryu, S. H. Lee, D. H. Nam, Prof. C. B. Park
Department of Materials Science and Engineering
Korea Advanced Institute of Science and Technology (KAIST)
335 Science Road, Daejeon 305–701, Republic of Korea
E-mail: parkcb@kaist.ac.kr

DOI: 10.1002/adma.201004576

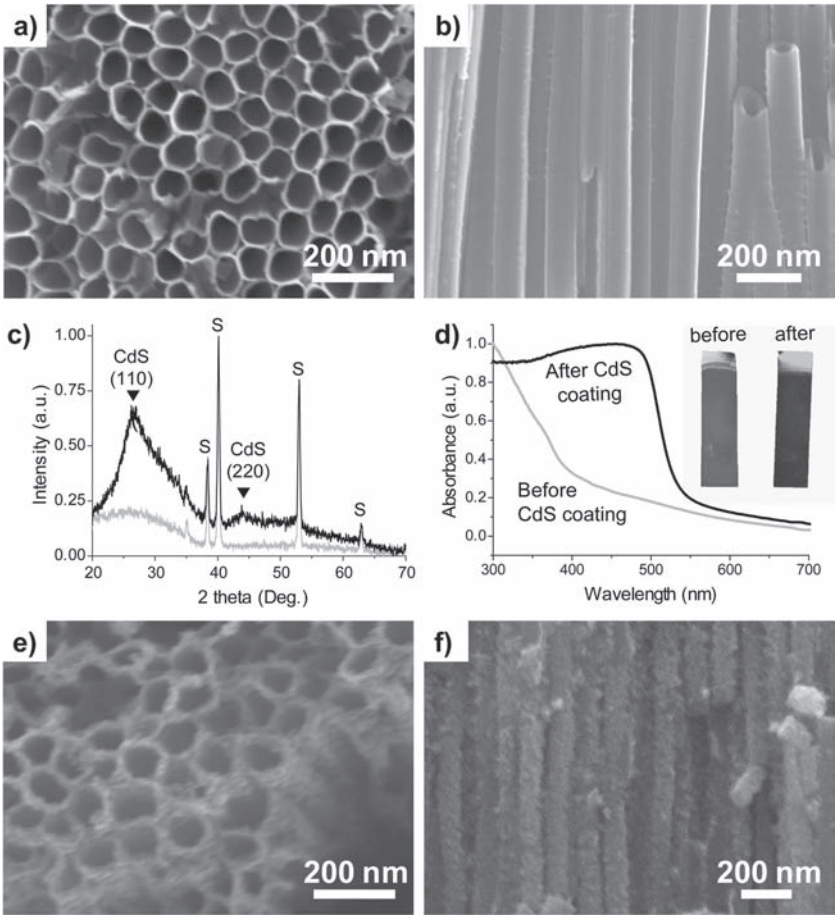

Figure 1. Characterization of anodized TiO_2 nanotubes by SEM (a,b,e,f), XRD (c), and UV-visible spectroscopy (d) before and after CdS coating. TiO_2 nanotubes were prepared by anodization at 60 V for 1 h and then coated with CdS quantum dots using the SILAR method. Before the coating, TiO_2 nanotubes had a smooth surface and were found to be amorphous ((c), grey solid line) without absorbance in the visible light range ((d), grey solid line). After the coating, TiO_2 nanotubes exhibited increased roughness (e,f) with absorbance in the visible light range ((d), black solid line) by the formation of CdS nanoparticles ((c), black solid line). In the XRD patterns (c), "S" indicates substrate peak. The inset in (d) is photograph of a TiO_2 nanotube film before and after the coating.

the Experimental Section. Throughout the photoregeneration tests, the ratio of the reactor volume to the apparent surface area of the photoelectrode was kept constant at 1 cm^3 per cm^2. It was found that the larger the pore diameter (94.9 nm vs 63.4 nm, Figures 2a,b), the higher the photoregeneration yield (50.3% vs 5.35% for 2 h, Figure 2d). This result was true even with similar surface area (581 cm^2 vs 485 cm^2 per cm^2 of substrate), which implies that the diffusion of the reaction species is a critical factor for optimizing the photoregeneration system. The maximum regeneration efficiency was achieved by a TiO_2–CdS NT film prepared by four cycles (4× TiO_2–CdS) of a SILAR process, independent of the dimensions of the TiO_2 nanotubes; this result created a bell-shaped plot of the number of CdS coating cycle versus NADH regeneration yield (Figure 2e). We speculate that such behavior results from a compromise between a larger amount of light absorption and a lower efficiency of charge separation, as well as limited diffusion by channel blocking (Figure S4, Supporting Information) at a higher degree of CdS loading. According to a recent report,[33] smaller quantum dots inject electrons into TiO_2 more efficiently than larger ones. The larger the bandgap, the more negative the position of the CB edge of CdS; thus, the higher the driving force for electron injection (i.e., the difference between the position of the CB edges of CdS and TiO_2). To support the hypothesis that efficient charge separation in TiO_2–CdS nanotubes can enhance the efficiency of NADH photoregeneration, a CdS-coated Al_2O_3 nanotube (Al_2O_3–CdS) film was prepared using a commercially available anodized aluminum oxide membrane (Figure S5, Supporting Information). Despite much larger dimensions (211 nm in pore diameter and 60 μm in length on average) and surface area (1131 cm^2 per cm^2 of substrate), the Al_2O_3–CdS NT film exhibited much lower regeneration yield (Figure 2e), which is attributed to a higher degree of charge recombination (**Figure 3**). L-glutamate was successfully synthesized by coupling the NADH photoregeneration with a redox enzyme (i.e., glutamate dehydrogenase (GDH))-catalyzed reductive amination reaction (Figure 2f).

We further attempted to optimize the photoregeneration system by controlling the crystallinity of the TiO_2 nanotubes by heat treatment. It was anticipated that the higher the crystallinity of TiO_2, the lower the density of defects acting as a site of electron trapping; thus, the higher the regeneration efficiency. A TiO_2 nanotube film was prepared by anodizing Ti foil at 60 V for 1 h and then annealing at room temperature, 150 °C, 300 °C, and 450 °C for 2 h in air. The crystallization of TiO_2 was investigated by multiple analytical tools such as SEM (**Figures 4**a–c), XRD (Figure 4d), and Raman spectroscopy (Figure S6, Supporting Information). After the annealing at high temperatures, the tubular morphology of TiO_2 nanotubes remained; however, the initially smooth surface of amorphous TiO_2 became highly rugged (Figures 4a–c) by the crystallization of TiO_2 from amorphous to anatase phase (Figure 4d and Figure S6, Supporting Information). Note that annealing at temperatures higher than 600 °C disrupted tubular structure and caused a phase transformation to the rutile phase (data not shown). The sizes of TiO_2 nanocrystallites can be estimated by using XRD patterns (Figure 4d) and Scherrer's equation[34] or using a shift of the E_g band peak position in Raman spectra[35] (Figure S6, Supporting Information), as listed in Table S2 (Supporting Information). TiO_2 nanotubes that had different crystallinities were then coated with CdS for NADH photoregeneration (Figures 4e,f). With an increase in the annealing temperature up to 300 °C (and thus increase in the size of TiO_2 nanocrystallites), the photoregeneration efficiency increased by ≈1.5 times from 49.9% to 75.2% for 4× TiO_2–CdS

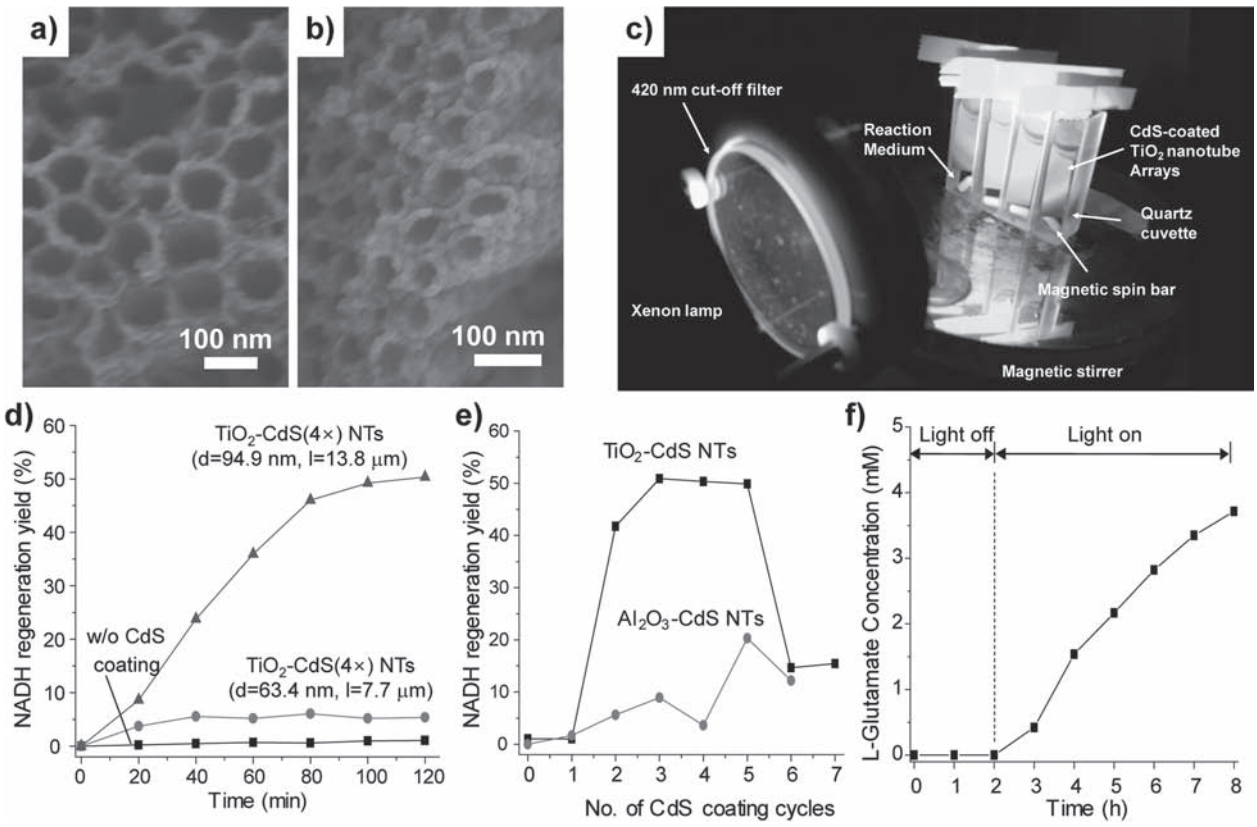

Figure 2. Photoenzymatic synthesis of L-glutamate using CdS quantum-dot-sensitized TiO_2 nanotube arrays. a,b) SEM images of CdS-coated TiO_2 nanotubes (TiO_2–CdS NT). TiO_2–CdS NTs were prepared by anodizing Ti foil at 60 V for 1 h (a) or 30 V for 12 h (b), followed by coating with CdS nanoparticles by 4 cycles of a SILAR process. c) Experimental setup for the photoenzymatic reaction. d) Photoregeneration of NADH using TiO_2–CdS NTs with different dimensions (*d* is the pore diameter, *l* is the tube length). e) Comparison between the efficiencies of NADH photoregeneration by TiO_2–CdS NTs and Al_2O_3–CdS NTs with different degrees of CdS loading. f) Photoenzymatic synthesis of L-glutamate by coupling GDH biocatalysis with photoregeneration of NADH on a TiO_2–CdS NT film.

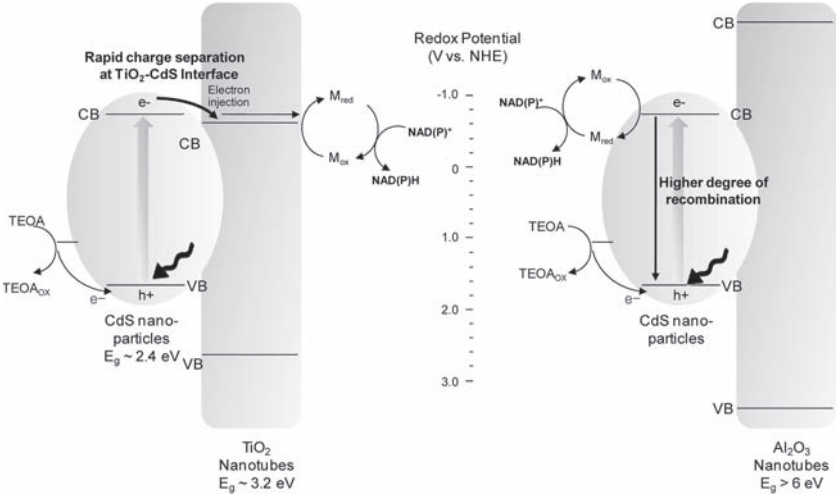

Figure 3. Suggested mechanism for higher efficiency of NADH photoregeneration by a TiO_2–CdS nanotube film than a Al_2O_3–CdS nanotube film. In the TiO_2–CdS nanotube film, electron injection from CdS to TiO_2 is thermodynamically favored due to more negative conduction band potential of CdS than TiO_2, suppressing electron–hole recombination dominantly occurring in a nanosized semiconductor particle. In a Al_2O_3–CdS nanotube film, on the contrary, excited electrons can recombine with the hole at higher degree than in TiO_2–CdS film, which lowers the efficiency of NADH photoregeneration. M indicates a $[Cp^*Rh(bpy)H_2O]^{2+}$ complex.

nanotube films. This result is attributed to the increased electron lifetime by crystallization of TiO_2.[36] Unexpectedly, however, the efficiency decreased to 54.4% for samples treated at 450 °C. The formation of larger crystals should decrease the surface area according to a recent report,[37] which may counter balance the effect of increased electron lifetime on the efficiency of cofactor photoregeneration.

To investigate the morphological effect of nanostructured TiO_2 film on the photoregeneration efficiency, a nanoparticulate TiO_2 film was fabricated for comparison. Nanoparticulate TiO_2 film (≈15 μm thick) was prepared by the doctor-blade method[38] using a paste composed of commercially available TiO_2 nanoparticles and titanium tetraisopropoxide (TTIP). The prepared TiO_2 film was then annealed at room temperature overnight and at 150 °C for 10 min to enhance the mechanical stability by interconnecting nanoparticles to each other through hydrolysis and condensation of TTIP. The formation of the stable

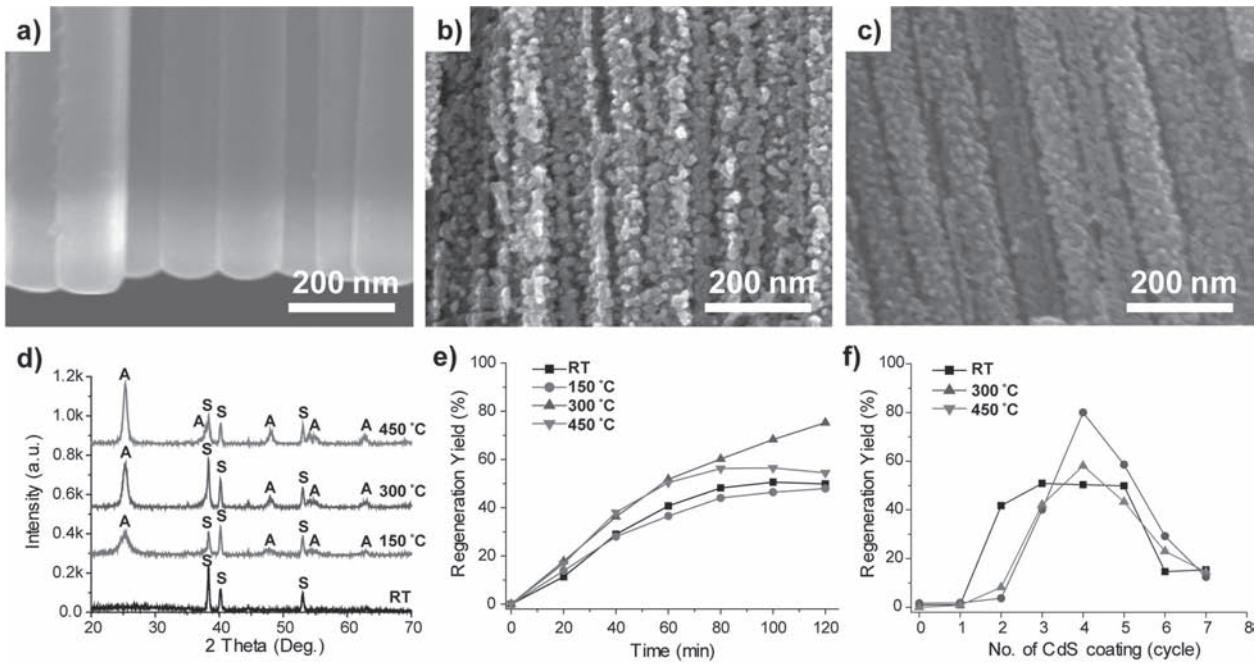

Figure 4. Effect of the crystallinity of TiO_2 nanotubes on NADH photoregeneration by TiO_2–CdS NTs. TiO_2 nanotubes were prepared by anodization at 60 V for 1 h and annealed at different temperatures to control the crystallinity of TiO_2 nanotubes. The crystallization of TiO_2 nanotubes were studied by SEM at different temperatures (RT (a), 300 °C (b), 450 °C (c)) and XRD (d). S and A indicate substrate and anatase TiO_2 peaks, respectively. TiO_2–CdS NT films with different crystallinities of TiO_2 (e) and different degrees of CdS loading (f) were examined to optimize the photoregeneration of NADH using a TiO_2–CdS NT film.

nanoparticulate TiO_2 film was confirmed using SEM (**Figure 5**a,b), XRD (Figure S7a, Supporting Information), and Raman spectroscopy (Figure S6 and S7b, Supporting Information). TiO_2 in the nanoparticulate film was nanocrystalline anatase with an estimated size comparable to that in the nanotubular film annealed at 450 °C (9.3 nm vs 10.4 nm, see Table S2, Supporting Information). Both nanoparticulate and nanotubular TiO_2 films were then coated with CdS and tested for cofactor regeneration. It was found that the nanotubular TiO_2 film can regenerate NADH at least four times more efficiently than its nanoparticulate counterpart (Figure 5c). As expected from the above discussion, more efficient diffusion of the reaction species in the nanotubular film was thought to be mainly responsible for the higher efficiency of NADH photoregeneration (Figure 5d). According to previous reports,[24,26] directional morphology of the tubular film enables better collection and transport of electrons than the particulate film, which suggests that the difference between electron transport behaviors in the tubular and particulate TiO_2 films can also affect NADH photoregeneration.

The nanostructured TiO_2–CdS photoelectrode has many advantages for cofactor

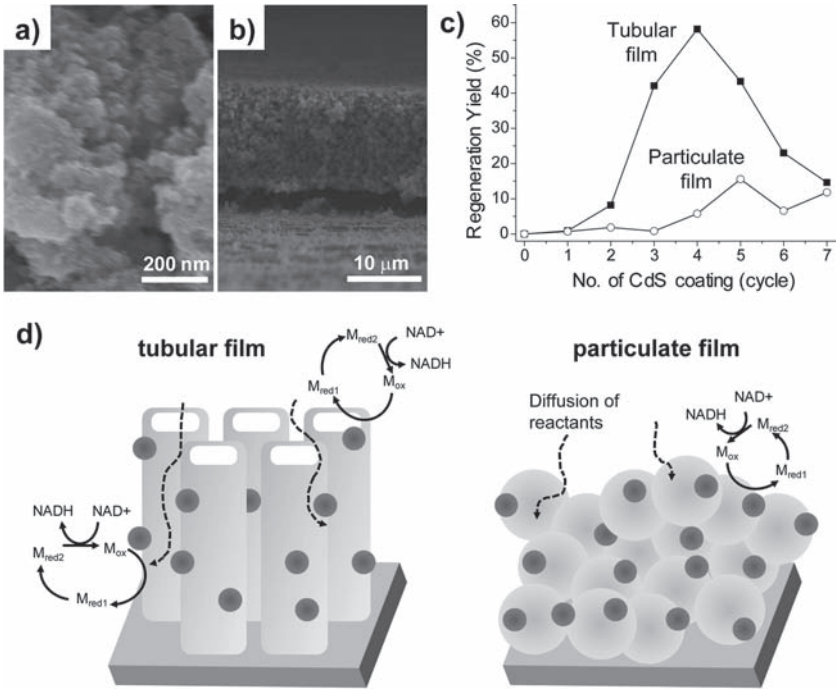

Figure 5. Comparison between efficiencies of NADH photoregeneration by particulate and tubular TiO_2-CdS nanocomposite films. a,b) SEM images of a nanoparticulate TiO_2 film prepared by the doctor-blade method. c) Photoregeneration of NADH using a nanoparticulate (open circles) and a nanotubular (filled square) TiO_2–CdS film. d) Schematic illustration explaining the higher efficiency of NADH photoregeneration obtained with a TiO_2–CdS NT film.

regeneration. For example, conventional biocatalytic regeneration methods have critical problems such as by-product formation and the requirement of a secondary enzyme, which cause an increase in regeneration cost and pose a significant hurdle for their practical implementation.[10–12] To avoid such problems, researchers investigated electrochemical[13–15] methods that use the reducing power of electrons supplied from the electrode connected to an external power supply for cofactor regeneration. Compared to the electrochemical methods, photochemical regeneration is considered to be more promising in terms of scale-up of the reactor and energy consumption because it utilizes a renewable energy source (i.e., solar energy) without complex design and installation of the reactor for the external power supply. However, the photochemical regeneration method is still in its infancy and requires significant improvements in its design and efficiency.[39–41] In the present study, we have demonstrated that more efficient cofactor regeneration systems can be developed through rational design and engineering of nanostructured photosystems. For example, we found that the efficiency of NADH cofactor regeneration can be significantly enhanced by controlling the morphology/dimension of light-harvesting materials and integrating active components for efficient charge separation. We believe that these results provide a foundation for future studies on the design and engineering of photoenzymatic reaction systems for artificial photosynthesis.

In summary, we demonstrated bioinspired photoenzymatic synthesis of chiral compounds by coupling NADH photoregeneration on a TiO_2–CdS NT film with redox biocatalysis. We found that diffusion of the reaction species and efficient charge separation are key factors for optimizing photosystems for heterogeneous photoregeneration of cofactors through the investigation of effects of morphology and dimension of the TiO_2 nanotubes and hybridization of CdS with TiO_2 on the efficiency of NADH photoregeneration. Our findings provide a new strategy for developing more efficient artificial photosynthetic systems via rational design and engineering of photosystems.

Experimental Section

Materials: All chemicals, including triethanolamine (TEOA), NAD^+, $CdSO_4$, $Na_2S{\cdot}9H_2O$, ethylene glycol, NH_4F, anatase TiO_2 nanopowder (Cat. No. 637254), titanium tetraisopropoxide (TTIP), Ti foil (0.127 mm thick), α-ketoglutarate, and glutamate dehydrogenase (GDH), were purchased from Sigma-Aldrich (St. Louis, MO). Porous graphite felt (GF-S6) was purchased from Electrolytica, Inc. (Amherst, NY). Anodized Al_2O_3 membrane filter (Anodisc 47) was obtained from Whatman, Ltd. (Clifton, NJ, USA). The electrolyte solution for anodization of Ti was prepared by dissolving NH_4F at 0.3 wt% in solution mixture of ethylene glycol (98 vol%) and water (2 vol%). TiO_2 nanoparticle paste was prepared by dissolving 3.5 g of TiO_2 nanopowder in 15 mL of ethanol, followed by homogeneous mixing with TTIP (0.5 mL). $[Cp^*Rh(bpy)H_2O]^{2+}$ was synthesized according to previous studies [29,30]

Synthesis of Nanotubular and Nanoparticulate TiO_2 Films: TiO_2 nanotubes were prepared by anodization. Details of the experiment can be found elsewhere.[25,26] Before anodization, Ti foil was cut into sizes of 10 mm × 40 mm and degreased by ultrasonication in acetone and ethanol for 30 min. The anodization of Ti was carried out in a two-electrode configuration by using Ti foil as a working electrode and porous graphite felt as a counter electrode at 60 V for 1 h or at 30 V for 12 h. As-anodized TiO_2 nanotubes were ultrasonicated in a water/ethanol mixture to remove surface debris formed during the anodization. The average diameter and length of the TiO_2 nanotubes and calculated surface area of TiO_2 per cm^2 of Ti substrate were 94.9 ± 11.1 nm, 13.8 ± 1.1 μm, and 581 cm^2 for samples anodized at 60 V for 1 h, and 63.4 ± 5.8 nm, 7.7 ± 0.3 μm, and 485 cm^2 for samples anodized at 30 V for 12 h, respectively. For crystallization of TiO_2 nanotubes, as-anodized samples were annealed at room temperature (RT), 150 °C, 300 °C, and 450° for 2 h in air with a constant heating and cooling rate of 1 °C min^{-1}. Nanoparticulate TiO_2 film was fabricated by the doctor-blade method.[38] The TiO_2 nanoparticle paste was uniformly coated in a thickness of 15 μm on Ti foil by using a doctor-blade coater. The nanoparticulate film was then annealed at room temperature overnight and at 150 °C for 10 min to enhance its mechanical stability by interconnecting TiO_2 nanoparticles through hydrolysis and condensation of TTIP.

Decoration of Nanotubular and Nanoparticulate TiO_2 Films: A TiO_2 nanotube film prepared by anodization, a TiO_2 nanoparticle film prepared by the doctor-blade method, and a Al_2O_3 nanotube film prepared by using commercially available anodic aluminum oxide membrane were coated with CdS nanoparticles using the SILAR method. One cycle of the SILAR process consisted of sequential treatments with 0.1 M $CdSO_4$, deionized water, 0.1 M Na_2S, and deionized water for 10 min each. The degree of CdS loading was controlled by repeating the SILAR process (0–7 times).

Characterization: The microstructure of the nanostructured films was observed with an S-4800 field emission scanning electron microscope (Hitachi High-technologies CO., Japan). Absorbance spectra of TiO_2 nanotubes before and after CdS coating were measured by using a V/650 spectrophotometer (Jasco, Inc., Tokyo, Japan) in diffuse reflectance mode. The optical bandgap was estimated by Tauc's extrapolation method.[31] The crystal structure of the nanostructured TiO_2 film was investigated using a D/MAX-RC thin-film X-ray diffractometer (Rigaku Co., Japan) and a LabRAM UV-vis-NIR high-resolution dispersive Raman microscope (Horiba Jobin Yvon, France). The XRD patterns were collected under the following conditions: scan speed, 1° min^{-1}; Cu Kα radiation, $\lambda = 1.5418$ Å; scan range, 20°–70°. The Raman spectra were measured with a resolution of 4 cm^{-1} in the spectral range of 100–700 cm^{-1}. The size of the anatase nanocrystallites in nanostructured TiO_2 films was calculated by using a full width at half-maximum (FWHM) of the anatase (101) peak and Scherrer's equation[34] or using a shift of the E_g band peak position in Raman spectra.[38]

NADH Photoregeneration and Photoenzymatic Synthesis of L-Glutamate: Photoregeneration of NADH was carried out by immersing the nanocomposite film into reaction medium upon irradiation with a xenon lamp (450 W) through a 420-nm cut-off filter (see also Figure 2c). The reaction medium (pH 7.5) was composed of NAD^+ (1 mM), $[Cp^*Rh(bpy)H_2O]^{2+}$ (0.25 mM), TEOA (15 w/v%), and phosphate buffer (100 mM); 3 mL of the medium was filled in a quartz cell. Throughout the experiment, the ratio of reactor volume to apparent surface area of photoelectrode was maintained at 1 cm^3 per cm^2. During the photoregeneration of NADH, the concentrations of NAD^+ and NADH were estimated by measuring the absorbance of reaction medium at 260 and 340 nm, respectively (see Figure S8, Supporting Information). Note that the absorption coefficient of NADH at 340 nm is 6.22 mM^{-1} cm^{-1}. For the photoenzymatic synthesis of L-glutamate, GDH-catalyzed reductive amination reaction was coupled with photoregeneration of NADH from NAD^+ using a TiO_2–CdS nanotube film. The reaction medium for the photoenzymatic reaction consisted of NAD+ (1 mM), $[Cp^*Rh(bpy)H_2O]^{2+}$ (0.5 mM), α-ketoglutarate (5 mM), $(NH_4)_2SO_4$ (100 mM), GDH (40 U), TEOA (15 w/v%), and 0.1 M phosphate buffer (pH 7.4).

Supporting Information

Supporting Information is available from the Wiley Online Library or from the author.

Acknowledgements

This study was supported by grants from the National Research Foundation (NRF) via National Research Laboratory (R0A-2008–000-20041–0), Engineering Research Center (2008–0062205), and Converging Research Center (2009–0082276) programs. This research was also partially supported by the KAIST Energy Environment Water Sustainability (EEWS) Initiative.

Received: December 14, 2010
Published online: February 11, 2011

[1] A. Schmid, J. S. Dordick, B. Hauer, A. Kiener, M. Wubbolts, B. Witholt, *Nature* **2001**, *409*, 258.
[2] D. J. Pollard, J. M. Woodley, *Trends Biotechnol.* **2007**, *25*, 66.
[3] W. Hummel, *Trends Biotechnol.* **1999**, *17*, 487.
[4] V. B. Urlacher, S. Eiben, *Trends Biotechnol.* **2006**, *24*, 324.
[5] R. N. Patel, *Coord. Chem. Rev.* **2008**, *252*, 659.
[6] H. Zhao, W. A. Van Der Donk, *Curr. Opin. Biotechnol.* **2003**, *14*, 583.
[7] R. Wichmann, D. Vasic-Racki, *Adv. Biochem. Eng./Biotechnol.* **2005**, *92*, 225.
[8] H. Hollmann, K. Hofstetter, A. Schmid, *Trends Biotechnol.* **2006**, *24*, 163.
[9] S. M. A. de Wildeman, T. Sonke, H. E. Schoemaker, O. May, *Acc. Chem. Res.* **2007**, *40*, 1260.
[10] Z. S. Shaked, G. M. Whitesides, *J. Am. Chem. Soc.* **1980**, *102*, 7104.
[11] J. Lutz, V. V. Mozhaev, Y. L. Khmelnitsky, B. Witholt, A. Schmid, *J. Mol. Catal. B: Enzym.* **2002**, *19–20*, 177.
[12] T. W. Johannes, R. D. Woodyer, H. Zhao, *Biotechnol. Bioeng.* **2007**, *96*, 18.
[13] F. Hollmann, A. Schmid, E. Steckhan, *Angew. Chem. Int. Ed.* **2001**, *40*, 169.
[14] H.-K. Song, S. H. Lee, K. Won, J. H. Park, J. K. Kim, H. Lee, S.-J. Moon, D. K. Kim, C. B. Park, *Angew. Chem. Int. Ed.* **2008**, *47*, 1749.
[15] S. H. Lee, K. Won, H.-K. Song, C. B. Park, *Small* **2009**, *5*, 2162.
[16] A. F. Collings, C. Critchley, *Artifical photosynthesis: from basic biology to industrial application,* Wiley-VCH, Weinheim, Germany **2005**.
[17] R. E. Blankenship, *Molecular mechanisms of photosynthesis,* Blackwell Science Ltd, Oxford, UK **2002**.
[18] L. Vayssieres, *On solar hydrogen & nanotechnology*, John Wiley & Sons, Singapore **2009**.
[19] B. O'Regan, M. Gratzel, *Nature* **1991**, *353*, 737.
[20] B. E. Hardin, E. T. Hoke, P. B. Armstrong, J.-H. Yum, P. Comte, T. Torres, J. M. Frechet, M. Khaja, M. K. Nazeeruddin, M. Gratzel, M. D. McGehee, *Nat. Photonics* **2009**, *3*, 406.
[21] O. K. Varghese, M. Paulose, C. A. Grimes, *Nat. Nanotechnol.* **2009**, *4*, 592.
[22] D. R. Baker, P. V. Kamat, *Adv. Funct. Mater.* **2009**, *19*, 805.
[23] P. V. Kamat, *J. Phys. Chem. C* **2007**, *111*, 2834.
[24] P. V. Kamat, *J. Phys. Chem. C* **2008**, *112*, 18737.
[25] J. M. Macak, H. Tsuchiya, L. Taveira, S. Aldabergerova, P. Schmuki, *Angew. Chem. Int. Ed.* **2005**, *44*, 7463.
[26] K. Shankar, J. I. Basham, N. K. Allam, O. K. Varghese, G. K. Mor, X. Feng, M. Paulose, J. A. Seabold, K.-S. Choi, C.A. Grimes, *J. Phys. Chem. C* **2009**, *113*, 6327.
[27] W.-T. Sun, Y. Yu, H.-Y. Pan, X.-F. Gao, Q. Chen, L.-M. Peng, *J. Am. Chem. Soc.* **2008**, *130*, 1124.
[28] Y. Bessekhouad, D. Robert, J. V. Weber, *J. Photochem. Photobiol. A* **2004**, *163*, 569.
[29] H. C. Lo, O. Buriez, J. B. Kerr, R. H. Fish, *Angew. Chem. Int. Ed.* **1999**, *38*, 1429.
[30] F. Hollmann, B. Witholt, A. Schmid, *J. Mol. Catal. B: Enzym.* **2003**, *19–20*, 167.
[31] J. Tauc, A. Menth, *J. Non-Cryst. Solids* **1972**, *8*, 569.
[32] Y. Wang, N. Herron, *Phys. Rev. B* **1990**, *42*, 7253.
[33] I. Robel, M. Kuno, P. V. Kamat, *J. Am. Chem. Soc.* **2007**, *129*, 4136.
[34] B. D. Cullity, S. R. Stock, *Elements of X-ray diffraction*, 3rd ed. Prentice Hall, NJ **2001**.
[35] W. F. Zhang, Y. L. He, M. S. Zhang, Z. Yin, Q. Chen, *J. Phys. D: Appl. Phys.* **2000**, *33*, 912.
[36] S. Nakade, M. Matsuda, S. Kambe, Y. Saito, T. Kitamura, T. Sakata, Y. Wada, H. Mori, S. Yanagida, *J. Phys. Chem. B* **2002**, *106*, 10004.
[37] S. Biswas, A. Majumder, M. F. Hossain, T. Takahashi, Y. Kubota, A. Fujishima, *J. Vac. Sci. Technol. A* **2008**, *26*, 678.
[38] D. Zhang, T. Yoshida, T. Oekermann, K. Furuta, H. Minoura, *Adv. Funct. Mater.* **2006**, *16*, 1228.
[39] C. B. Park, S. H. Lee, E. Subramanian, B. B. Kale, S. M. Lee, J.-O. Baeg, *Chem. Commun.* **2008**, 5423.
[40] D. H. Nam, S. H. Lee, C. B. Park, *Small* **2010**, *6*, 922.
[41] Q. Shi, D. Yang, Z. Jiang, J. Li, *J. Mol. Catal. B* **2006**, *43*, 44.